Available online at www.sciencedirect.com

jmr&t Journal of Materials Research and Technology

journal homepage: www.elsevier.com/locate/jmrt

Original Article

Research of friction materials applicable to the multi-disc brake concept

Daniel Varecha [a,*], *Jozef Bronček* [a], *Róbert Kohár* [a], *František Nový* [b], *Martin Vicen* [b], *Norbert Radek* [c]

[a] *Faculty of Mechanical Engineering, Department of Design and Machine Elements, University of Žilina, Univerzitná 8215/1, Žilina, 010 26, Slovak Republic*

[b] *Faculty of Mechanical Engineering, Department of Materials Engineering, University of Žilina, Univerzitná 8215/1, Žilina, 010 26, Slovak Republic*

[c] *Faculty of Mechatronics and Machine Design, Centre for Laser Technologies of Metals, Kielce University of Technology, Aleja Tysiąclecia Państwa Polskiego 7, Kielce, 25 314, Poland*

ARTICLE INFO

Article history:
Received 7 April 2021
Accepted 22 June 2021
Available online 26 June 2021

Keywords:
ESD coating
WC-Cu
Friction materials
AGV
Simulation

ABSTRACT

This manuscript is focused on the investigation of tribological and thermodynamic parameters of the coated C45 steel substrate. A metallic coating of the WC-Cu base was applied on the C45 steel substrate using electro-spark deposition (ESD) coating technology. Three types of experimental WC-Cu coatings with different ratio of chemical elements were deposited on the surface of the C45 steel substrate using WC-Cu electrodes produced by the powder metallurgy route. Each sample had a different ratio of WC-Cu chemical elements. Subsequently, the friction factor (f) and the total wear of the sample were examined in a tribological laboratory. The objectively most suitable sample in terms of friction factor and service life was subjected to a braking simulation in Matlab® software together with three other commercial friction materials. A mathematical model of Newton's equations of motion was used to simulate braking. The last phase of the research was focused on the thermodynamic parameter during automatically guided vehicle (AGV) braking. The tribological results of tested coatings showed that the most suitable combination of chemical elements in the WC-Cu type ESD coating is the WC50–Cu50 ratio. The simulation of non-stationary heat conduction process in the brake system revealed that the most suitable thickness of the steel brake disc should be at least 8.2 mm. Ultimately, this research will help the designer to choose the right procedures for designing a multi-disc brake system.

* Corresponding author.
E-mail address: daniel.varecha@fstroj.uniza.sk (D. Varecha).

https://doi.org/10.1016/j.jmrt.2021.06.061

1. Introduction

The authors present experimental research of friction materials used in the disc brake system of an automatically guided vehicle (AGV). AGVs are used in the field of logistics to transport production inputs and outputs in the production process. This type of vehicle is powered by a lithium-ion battery. The electric motor is used not only for movement but also for braking. It follows that the mileage of a vehicle is influenced not only by its design, but also by its driving style and operating factors [1,2]. The method of reducing kinetic energy by means of an electric motor with which the AGV is equipped is not effective in certain operating situations, e.g. during immediate braking. At present, a multi friction disc brake is being developed at the university workplace as part of experimental research, the aim of which is to streamline operation and increase the safety and efficiency of the AGV system [3]. The developed braking system is inspired by the braking system used in planetary gearboxes to shift gears [4]. Planetary gearboxes shift gears by braking the planetary rows using hydraulic energy. A design solution using the mounting of the bearing houses [5–7] into the wheel's body with the multi disc brake system was used according to publication [8]. The only difference is, that developed brake system uses a modern computer-controlled electric servo-engine, not a mechanical force induced by hydraulic energy.

The construction of the brake system (Fig. 2a) consists of two types of discs (spacers & washers). The first disc is frictional (Fig. 1a) and the second disc is made of steel for brake systems (Fig. 1b).

In the schematic representation of the brake system (Fig. 2b), all components are marked with positions. Where number 1. is the drive wheel shaft, 2. is the static part of the brake, 3. is the friction disc, 4. is the steel brake disc, 5. is the rotary pressure piston. The AGV is programmed for two operating modes. In the first operating mode it transports a cargo of 2020 kg and in the second operating mode it transports a cargo of 3020 kg including its own weight.

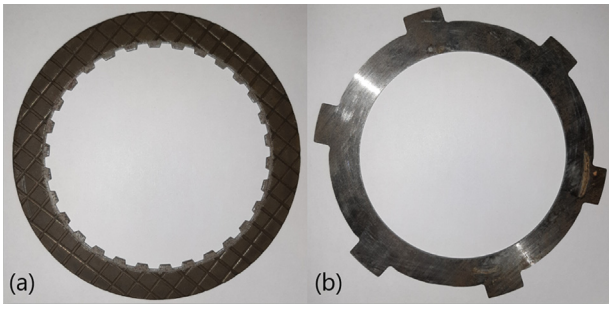

Fig. 1 – Friction disc (a), steel disc of the braking system (b) [30].

2. Overview of available friction materials

In the late 80s of the last century, organic paper material found application in brake systems of automatic planetary gearboxes as a friction material. It was applied in disc brakes and clutches for shifting gears. The brake system blocks the gears, and this way, shifting to the next gear [9]. A minor disadvantage of organic paper brake pads is that as the temperature rises from an ambient value of 22 °C to an operating temperature of 120–160 °C, the coefficient of friction decreases slightly, but with a preserved course of the curve [9]. According to publication [9], paper-based organic friction material has some properties that predispose it to the construction of brake systems. Its most remarkable property is the almost constant course of the coefficient of friction depending on the slip speed of the friction brake discs. In the area of low slip speeds, the coefficient of friction even decreases with decreasing slip speed. It follows from the above fact that the static coefficient of friction is lower than the

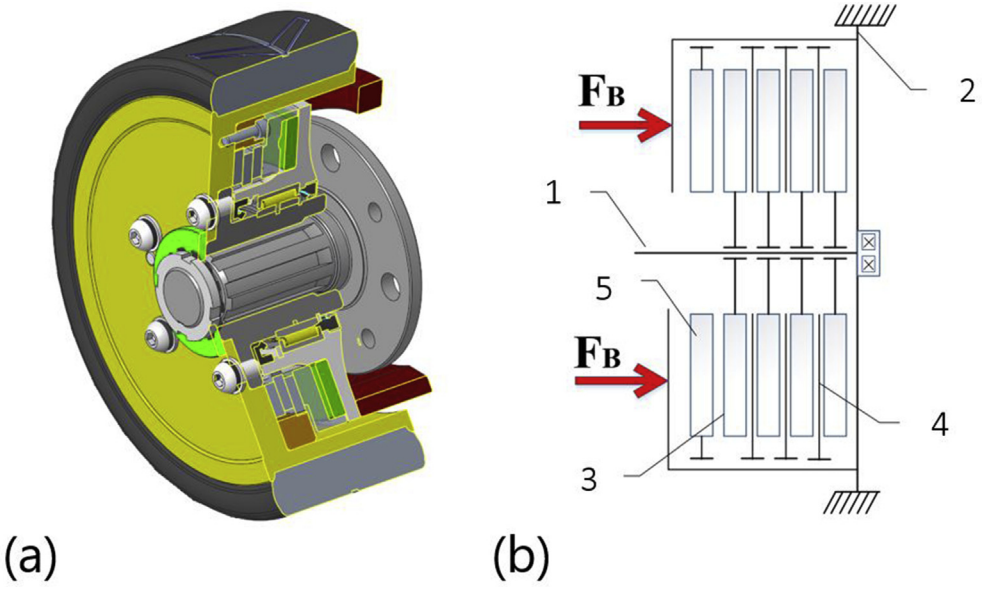

Fig. 2 – Graphical representation (a), schematic representation of the braking system (b).

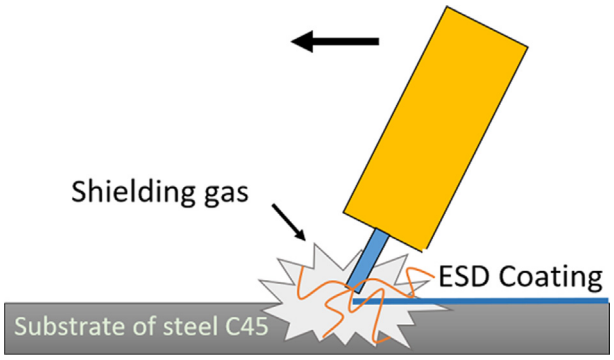

Fig. 3 – Electro-spark deposition coating [authors].

dynamic one [9]. The U.S. patent No. 4445190A states that an organic friction material based on chrysotile asbestos as the reinforcing base material and phenolic resin as a binder material with various friction-controlling agents have been used in the past [10]. The study also states that asbestos has excellent specific properties, but has recently been found to be harmful to human health and nature. Therefore, for obvious reasons, asbestos material has been replaced by synthetic aramid fibers [11]. The U.S. patent No. 3334998 and U.S. patent No. 3851118 describe another semi-metallic friction material which contains a metal as a base material and a resin as a bonding material. Manufacturers of friction components also produced friction materials from brass, copper and steel wool and used a resin binder in the past. Those materials are comparable in quality to the quality of the ceramic friction material. At the present time of the 21st century, brake systems are used in the automotive industry, the friction components of which are made up mostly of complex composite materials. In the publication [12] is stated that research has shown that the coefficient of friction and the way in which these friction materials are worn depend on several factors. The operational and material variables, the geometry of the friction surface, design, and last but not least, the environment in which they operate have a fundamental influence. The coefficient of friction of these composite friction materials is highest at the beginning of braking and decreases slowly over braking time. The reduction in the coefficient of friction is probably due to the decomposition of organic compounds in the brake materials. However, the coefficient of friction may later increase due to the formation of local carbonization on the worn surface [12]. In the field of ceramic friction materials, the following findings were found during development and research. The ceramic material has become a popular friction material due to its excellent heat resistance. The term "ceramics" refers to a very wide range of materials.

Table 1 – List of WC-Cu coatings used in the experiment [authors].

Specimen	Coating	WC	Cu
ESD-No.1	WC20–Cu80	20%	80%
ESD-No.2	WC50–Cu50	50%	50%
ESD-No.3	WC80–Cu20	80%	20%

Technically, it is an inorganic, non-metallic material that is created by the action of heat. The possibilities of using ceramic material are very wide because this material offers a wide range of available material properties and high quality. It can be used e.g. for the production of bricks, turbine blades for jet engines, or production of armoured armour for tanks. Currently, the ceramic brake pad consists of 20 or more components. The ceramic may be present in the brake pads in the form of particles or fibers. In the best brake pads, ceramic abrasive materials have two important utility functions. First, they directly affect the formation of friction and thus the performance of the brake pad. Second, they help clean rust and other impurities from the disc and create a consistent braking surface over the entire surface of the disc [13]. The research has shown that a brake system based on ceramic friction material shows significantly higher efficiency and durability than previously used organic and metallic friction materials. The material friction coefficient can be obtained e.g. by a reverse method described in [14]. Various experiments are currently underway with the coating of brake discs of vehicles. Porsche Surface Coated Brake (PSCB) is a technology that uses a revolutionary brake disc coating to provide excellent brake performance. The brake system based on technology (PSCB) was tested by automotive company Porsche on model Cayenne. After thousands of kilometers were the brakes on the new Porsche Cayenne test vehicles are still clean as a whistle [15,16]. The stated brake system performs almost as well as a ceramic brake system, but on the other side, it costs a lot of money. Other advantages are less wear than metallic brakes, almost no create brake dust and its brake system doesn't rust [15]. Manufacturing brake discs made entirely out of this material would have cost more than several sets of carbon-ceramic brakes. And we also don't currently have the technology to do that. The engineers decided to use standard brake discs with a tungsten carbide coating [15,16]. The tungsten carbide is applied using a state-of-the-art high-velocity oxy-fuel spraying process where the composite particles are shot onto the brake disc surface at supersonic speeds, resulting in an extremely dense, mirror-finish layer with a thickness of just 0.1 mm. Tungsten carbide has been extensively studied to date and has been found to be the perfect composite for the high demands of a vehicle's braking system [15,16]. Finally, it should be noted that tungsten and carbon form a mixed crystal, which is indeed the hardest material in the world after diamonds [15,16].

2.1. *Electro – spark deposition (ESD) coating*

Electro-spark deposition (ESD) is one of the methods that require a concentrated thermal energy flow [17]. The ESD technology was intensively used in the 1970s to apply hard materials to selected metals and their alloys, mainly to the steel surfaces (Fig. 3). Using ESD technology, different

Table 2 – Chemical composition (in wt. %) and hardness HV of the C45 steel substrate.

C	Si	Mn	P	S	Cr	Fe	HV
0.485	0.206	0.725	0.007	0.0033	0.068	Bal.	273

Table 3 – Chemical composition (in wt. %) and hardness HV of the friction ball.

C	Si	Mn	P	S	Cr	Mo	Ni	Fe	HV
1.226	0.363	0.502	0.003	0.0033	1.38	0.072	0.195	Bal.	774

chemical elements can be applied, either individually or as a combination of several elements. An example is the combination of molybdenum (Mo) with copper (Cu), or tungsten carbide (WC) and copper (Cu).

Various deposition techniques (ESD) are currently used, which are suitable for creating the surface micro-geometry of components. New machine parts can also be protected with ESD technology. Publication [17] states that the surface of the material treated with this technology is resistant to wear and corrosion. In case of wear of the coating, it is possible to regenerate the coating created by ESD technology. This technology is being carried out worldwide [17]. Among the best known companies interested in its use are NASA and the US Navy [17]. Anode electro erosion and spark discharges between the electrode and substrate lead to the material growth via formation of a surface layer with properties different from the base material's properties [18,19]. The publication [19] states that ESD coatings, which are post treated with laser remelting, have a higher adhesion to substrate than coatings without laser post treatment. The experimental tests [19] show a significant increase (about 26%) of the mean critical strength of the Cu–Mo coating after laser post treatment. The coating caused changes in the microhardness of the surface layers of the substrate material. After the application of the Cu–Mo coating, the micro-hardness of the surface layers increased significantly by 110%. After laser post treatment, the hardness of the coating was 51% higher than that of the base material of the substrate.

3. Experiment materials and methods

Within an experiment, test samples produced by machining were prepared. The proportional dimensions of the samples have been set at 30 × 70 × 8 mm. The WC-Cu wear resistant material was applied to the surfaces of the above mentioned samples by ESD technology. In the process of ESD coating application, WC-Cu electrodes with different ratio of chemical composition were used, resulting in a different chemical composition and friction properties of the coating. Three pairs of samples, each pair having a different chemical composition were prepared. The thickness of the WC-Cu coating is 0.3 mm. The exact ratio of the chemical elements of WC-Cu coatings for each sample is given in Table 1.

The authors in the publication [19] followed a similar procedure in the research, with a different ratio of WC-Cu chemical elements. Chemical composition of substrate (C45 steel) determined by spectrometer SPECTROMAXx operating on the principle of optical emission spectroscopy and its hardness measured in Vickers scale are given in Table 2.

Chemical composition of used friction ball (100Cr6 steel) and its hardness measured in Vickers scale are given in Table 3.

Tungsten carbide (WC) is an inorganic chemical compound consisting of an equal number of tungsten and carbon atoms. Tungsten carbide has approximately two times higher stiffness than steel. Its tensile modulus is about 550 GPa. The ratio of chemical elements has a significant impact on the friction properties of the WC-Cu coatings. It was found out [20] that with a lower tungsten carbide ratio, the WC-Cu coating loses its wear resistance. Opposite to that, a higher ratio results in a very tough coating, which is not suitable for brake systems, as a certain copper ratio produces balance in the friction factor. In an ideal ratio of tungsten carbide (WC) to copper (Cu), the coatings form thick layers characterized by a relatively high coefficient of friction. Our repeated research has shown that at the optimal ratio of WC-Cu chemical elements, the resulting coating is also characterized by excellent wear resistance. The coating formed by ESD technology has a very uneven

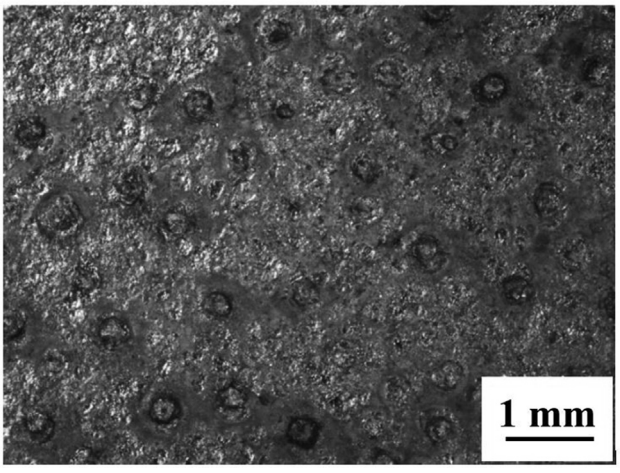

Fig. 4 – Surface structure of WC-Cu coatings [authors].

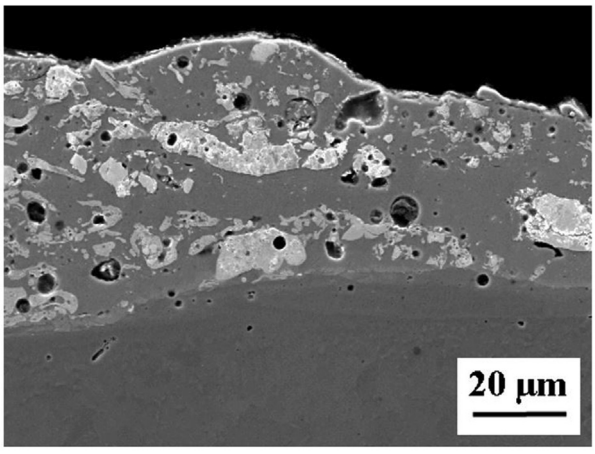

Fig. 5 – Microstructure of WC-Cu coatings in cross-section [authors].

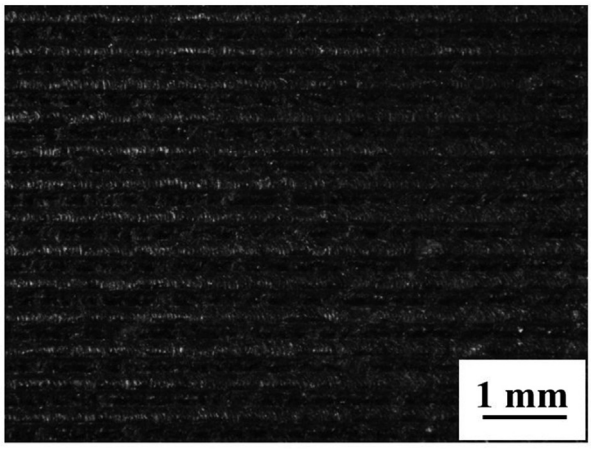

Fig. 6 – Surface structure of WC-Cu coatings after Laser Remelting [authors].

surface structure. Fig. 4 shows the surface character of the WC-Cu coating, before laser post treatment. Fig. 5 shows a cross-sectional view of the microstructure of the WC-Cu coating deposited on the C45 steel substrate before laser post treatment. The thickness of the obtained WC-Cu coating ranged from 36 to 60 μm, while the heat-affected zone (HAZ) in the C45 steel substrate ranged from 20 to 30 μm. Fig. 5 also reveals a clear boundary between the coating and the substrate and the pores in the coating.

From the comparison of surface character and microstructural features of WC-Cu coatings deposited by ESD technology before and after the laser post treatment following differences can be seen. The surface of laser post-treated coating has uniform character (Fig. 6). The laser post treatment homogenized chemical composition of deposited WC-Cu coatings, causing refinement of the structure (Fig. 7) and crystallization of nonequilibrium phases due to the occurrence of temperature gradients at high cooling rates.

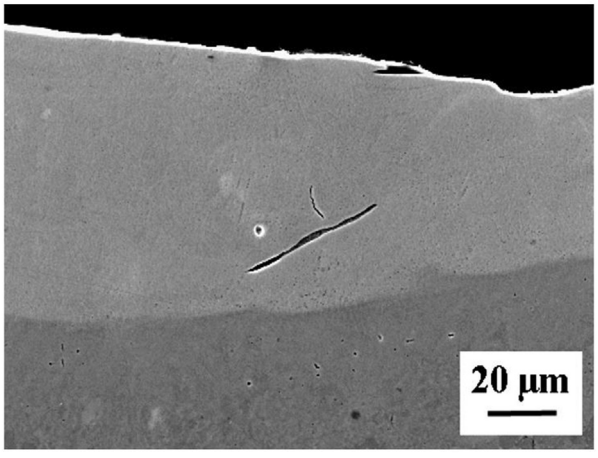

Fig. 7 – Microstructure of WC-Cu coatings after Laser Remelting [authors].

Moreover, the porosity and occurrence of microcracks in the WC-Cu coatings are near to zero after laser remelting post treatment. The thickness of laser post treated WC-Cu coatings remains unchanged (ranges from 42 to 64 μm). Also, the heat-affected zone (HAZ) is similar. It ranges also from 24 to 35 μm, but the carbon content in the fusion area of the HAZ zone is higher. All samples C45 steel substrate before ESD and samples with WC-Cu coatings without and with laser remelting post treatment were subjected to the hardness test. The microhardness of the coatings was examined according to the Vickers method. This type of hardness test is carried out according to the national standard EN ISO 6507–1. Individual measurements were made under a load of 0.5 N. The measured test results are given in Table 4.

Obtained results of hardness shows that the ESD process caused no significant changes in the micro-hardness of the substrate. The resulting micro-hardness of the C45 steel substrate was 273 HV0.5, with almost the same value being measured for the base material before ESD applying the WC-Cu coating (270 HV0.5). After applying the WC-Cu coating, there was obtained a coating with significantly higher micro-hardness. The micro-hardness of the WC-Cu coating reached 652 HV0.5. Obtained micro-hardness of the WC-Cu coatings was about 59% higher than that of the basic steel substrate after ESD in the HAZ. The laser post treatment caused a smoother character of the coating surface and had a favourable effect on the microstructural changes in the WC-Cu coating prepared using ESD. On the other hand, the experiment has confirmed that the laser post treatment of the coating slightly decreases the micro-hardness of the WC-Cu coating prepared using ESD. However, despite this fact, the WC-Cu coating after laser post treatment showed an increase in micro-hardness of 128%, compared to the base sample of the C45 steel substrate. The authors [20], recorded a decrease of micro-hardness about 9% in laser post treated coating. In this experiment, the micro-hardness decreased by approximately 5.2%.

4. Experimental methods

In the previous chapter, the results of the hardness of all tested samples are detailed. Another part of the research is focused on the samples without laser post treatment and their friction factor. To fulfil this task, a tribometer working on "Ball on Plate" principle was used (Fig. 8). The device performs a reversible movement of the ball tip with a sliding distance of 50 mm, given by its design. The normal force is

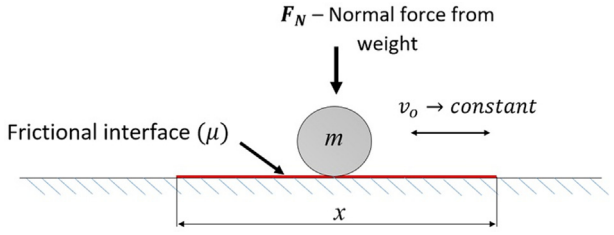

Fig. 8 – Schematic illustration of tribometer - method "Ball on Plate" [authors].

Table 4 – Results of the micro hardness tests for the WC-Cu coating.

Measured zones	Micro hardness HV 0.5 Measurement number			Mean value HV0.5	After laser post treatment			Mean value HV0.5
	1	2	3		1	2	3	
WC-Cu coating	631	675	651	652 ± 44	590	631	630	620 ± 20
WC-Cu HAZ	431	454	419	434 ± 35	394	421	403	406 ± 27
Substrate C45	264	284	271	273 ± 20	262	284	270	272 ± 22

generated by the weight applied to the tip. By adding or removing the weight, it is possible to change the normal force's magnitude and, ultimately, the friction pair's load. The friction force is measured by strain gauges during the test, and the measured data are sent to a computer for recording and further processing. It should be noted, tribological tests using the "Ball on disc" tribometer are model tests. Currently, tests are carried out using a "Block-on-Ring" tribometer. We are dealing then with a distributed contact of the friction pair. The tribological pairs consisted of experimentally prepared samples of C45 steel with WC-Cu coatings and a standard ball made of 100Cr6 bearing steel with a diameter of 5 mm and a hardness of 774 HV. The selected material of friction ball (100Cr6 bearing steel) is most suitable for this task due to its precise material properties and material integrity. The testing conditions were the same for all tribological pairs examined during the experimental measurement. The tribological tests were performed in the laboratory in the ambient air conditions without the use of lubrication. The velocity of the steel ball moving on the tested sample had a sine wave character ranging from v = 0–20 mm/s. The experiment took place in two-time phases. In the first phase, the test was set to time t = 6000 s. In the second phase of the experiment, the samples were monitored over a longer time t = 30,000 s (8.33 h). The friction pair load was constant with a value of normal force F_N = 5 N and 10 N for both time periods.

4.1. *Results of tribological test*

Coated WC-Cu samples were examined in two time periods. In the first phase, the experiment was set to a short time limit of 6000 s (1.6 h) and in the second phase it was set to 30,000 s (8.3 h). The impact of the load on the friction factor was monitored during the experiment. Fig. 9 shows diagrams of the friction factor over 6000 s recorded in the first phase of the investigation for samples with three variable WC-Cu ratios. A load force of 5 N was applied on the tribological pair. As can be seen, the sample with WC50–Cu50 coating reaches the highest value of friction factor. In the second phase of the investigation (Fig. 10), samples with the same three variable WC-Cu ratios as for the first phase of the investigation were used. As shown, the objective result of the friction factor can be obtained from a long-term experiment. From the comparison of results of the second phase of the investigation, it is clear that of the three samples with variable WC-Cu ratios, the WC50–Cu50 coating is objectively the most suitable in terms of friction factor. The friction factor ranged in an almost stable range of 0.70–0.78 throughout the experiment. The curve expressing the course of the friction factor for the WC20–Cu80 coating, resembles an irregular and fluctuating sine curve (Fig. 10). This is because of the structure of the coating consisting of 80% of copper (Cu) and 20% of tungsten carbide (WC).

The high content of copper (Cu) in the ESD coating structure reduces the wear resistance. A similar course of the curve can be seen in the results of the tribological pair, which was loaded with a force of 10 N (Fig. 11). The peak of the curve is due to the formation of local carbonization on the worn surface [21]. In case of long-term testing of WC80–Cu20 coating subjected to a 5N load (Fig. 10) the friction factor ranges in the interval 0.55–0.70. During the experiment, it was observed that the WC80–Cu2O coating, which was loaded with a force of 10 N, had a higher friction factor onset at the beginning of the test than the WC50–Cu50 coating.

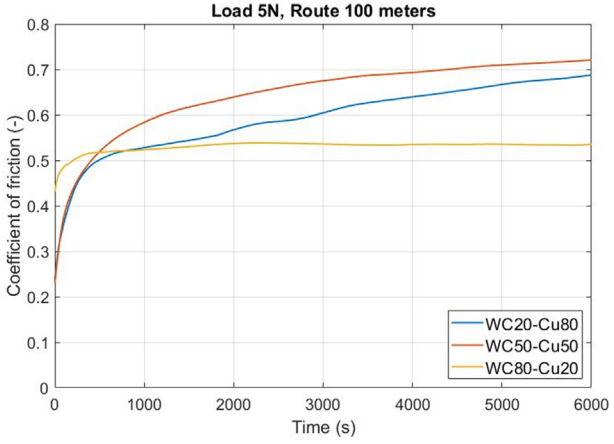

Fig. 9 – Test when loading a tribological pair 5N, distance 100 m.

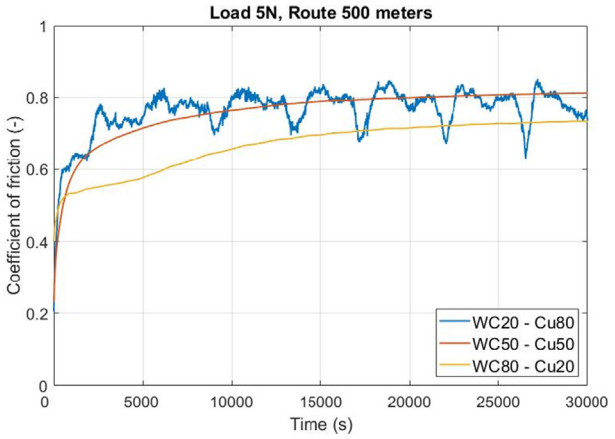

Fig. 10 – Test at load of tribological pair 5N, distance 500 m.

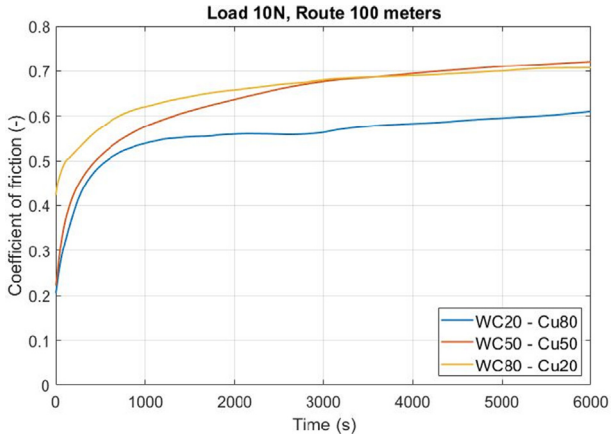

Fig. 11 – Test at load of tribological pair 10N, distance 100 m.

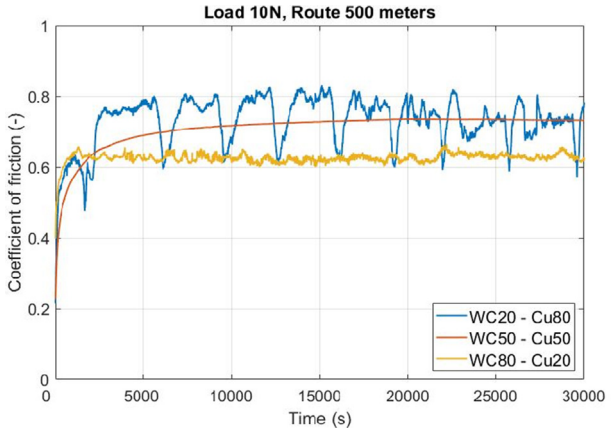

Fig. 12 – Test at load of tribological pair 10N, distance 500 m.

However, after 3000 s, the friction factor began to decrease gradually (Fig. 11). The sample with WC80–Cu20 coating, which was loaded with force of 10 N, showed a lower friction factor. It was in the range 0.60–0.65, and the course of the

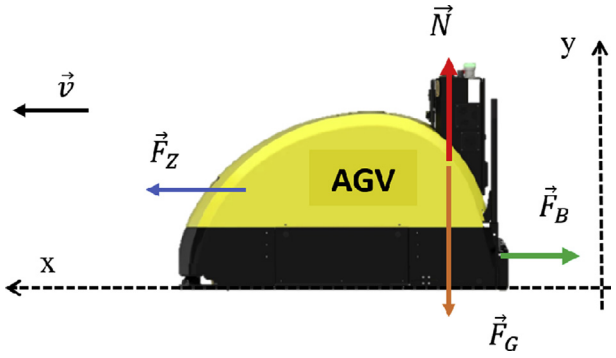

Fig. 14 – Acting forces on the AGV during braking [30].

Table 5 – Results from AGV braking simulation [authors].

	Coefficient of friction	Trajectory	Time
Organic	0.12	7.43 [m]	1.485 [s]
Metallic	0.31	5.66 [m]	1.131 [s]
Ceramic	0.42	5.03 [m]	1.005 [s]
ESD coating	0.65	4.07 [m]	0.814 [s]

curve oscillated in short and very dense waves (Fig. 12). This result was greatly influenced by the proportion of tungsten carbide in the coating. Based on comparison of the three sets of tribological data, it is clear that the coating WC50–Cu50, marked with the serial number ESD-No.2, has an optimal ratio between the service life and the friction factor. The set of measured tribological data was subsequently statistically evaluated, and the arithmetic mean of the friction factor was calculated (Eq. (1))

$$\overline{\mu}_{(WC50-Cu50)} = \frac{\sum_{i=1}^{n} x_i . n_i}{n}, [-] \quad (1)$$

where: $\overline{\mu}_{(WC50-Cu50)}$ is the final value of friction factor [-], x_i is the i-th value of the character [-], n_i is the number of measured values of the i-th character (with the same value) [-], n is the range of measured results [-].

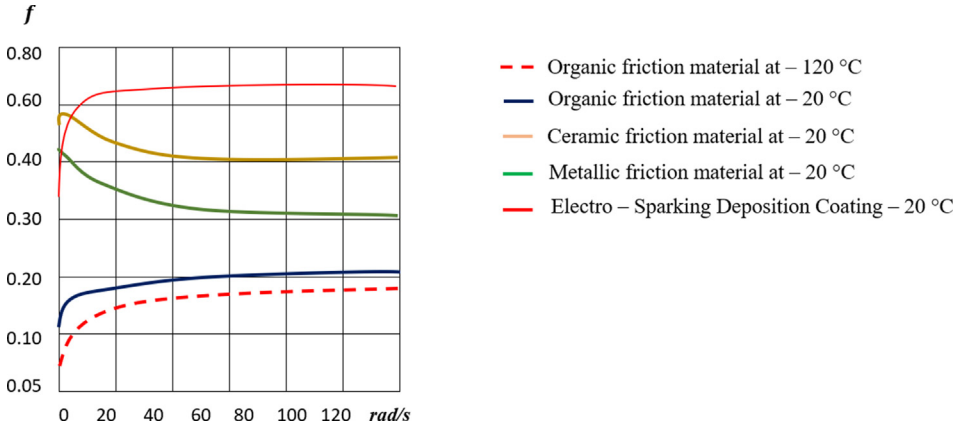

Fig. 13 – The course of the coefficient of friction of different materials [authors].

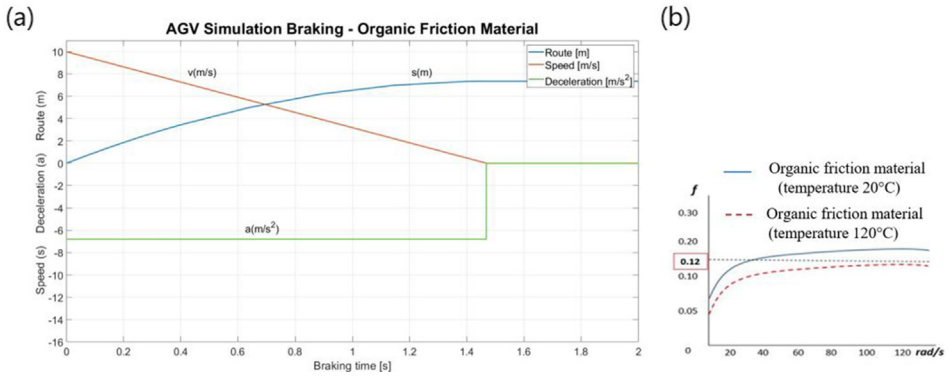

Fig. 15 – Brake system simulation - Organic material (a), Dependence of friction factor on wheel speed (b).

5. Simulation of AGV braking

The previous step investigated the tribological properties of three samples of the coated C45 steel substrate. The carried out tribological test shows that the sample with WC50–Cu50 coating has optimal physical and mechanical properties. The calculated average value of the friction factor was subsequently used in a computer simulation of AGV braking. Three other commercial friction materials were also subjected to braking simulations in order to compare them with ESD coated samples. The basic task of the simulation of the mechatronic system [22] is to obtain the interaction between the friction factors and the length of the braking distance at the theoretical level. The tribological diagram below shows the friction factor parameter of the individual materials used in the braking simulations (Fig. 13). The diagram shows that the curve of coated C45 steel substrate has a stable and linear course.

Matlab® computational software focused primarily on scientific and technical calculations, simulations, and a wide range of other applications was used to simulate braking. During the simulation, the AGV braking process was monitored from an operating speed of 10 m/s to a total stop. The script contained a set of sequential commands stored in the form of Newton's motion equations for speed (Eq. (3)), trajectory (Eq. (4)), and deceleration (Eq. (5)).

$$v(t) = \int ad = \int -\frac{F_B}{m} dt; [m/s] \tag{3}$$

$$s(t) = \int v(t)dt = \int \left(-\frac{F_B}{m}.t + v_0 \right) dt; [m] \tag{4}$$

$$a = -\frac{F_B}{m}; [m/s^2] \tag{5}$$

Newton's motion equations are derived from Fig. 14. The figure also shows the forces acting on the AGV during operation. The friction properties of metallic, ceramic, and organic friction material were compared with the friction properties of the ESD coatings on the C45 steel substrate during the simulation of AGV braking process (Table 5).

Due to a large amount of input mathematical data, a braking simulation was done only for the second operating mode (3020 kg load). The output data from the simulation are presented in the form of four diagrams, that express the influence of friction coefficient on the course of speed, trajectory, and deceleration of the AGV. The first graph describes the braking simulation course using a brake system based on organic paper material (Fig. 15).

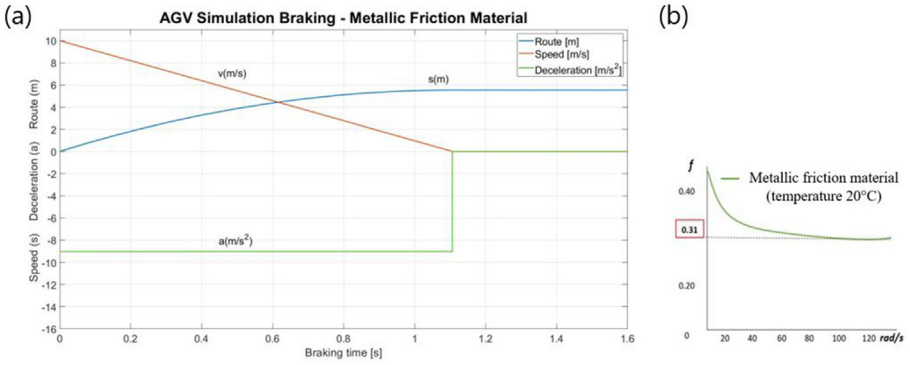

Fig. 16 – Brake system - Metallic material (a), Dependence of friction factor on wheel speed (b).

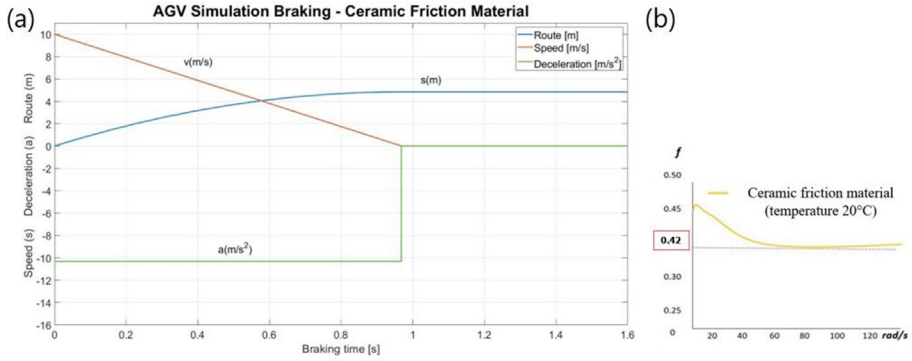

Fig. 17 – Brake system - Ceramic friction material (a), Dependence of friction factor on wheel speed (b).

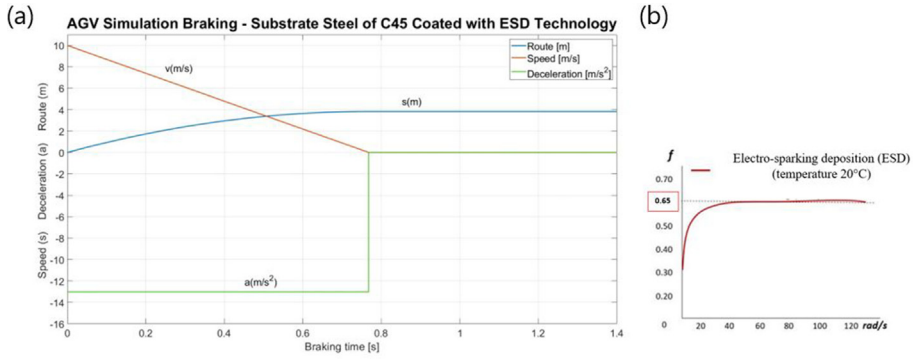

Fig. 18 – Brake system - ESD coated material (a), Dependence of friction factor on wheel speed (b).

The braking distance is the longest among all tested friction materials. The vehicle stopped after 7.43 m with a braking time of 1.485 s (Fig. 15a). This is due to the low value of the friction factor f = 0.12 (Fig. 15b). If the braking system were equipped with a metallic friction material with a coefficient of friction f = 0.31 (Fig. 16b), the braking distance of AGV would be 5.7 m. The time required to stop the AGV carrying weight of 3020 kg totally from a speed of 10 m/s is 1.18 s (Fig. 16a). Compare to the metallic friction material, the braking system based on ceramic friction material resulted in a lower braking distance during braking and shorter braking time. Under the considered operating conditions, AVG would stop at a distance of 5.03 m. The time in which the AVG stops totally was 1 s (Fig. 17a). However, the difference between both values of friction coefficient is not significant. The maximum value of the friction coefficient for ceramic and metallic materials reaches the peak at the beginning of braking and decreases subsequently until the friction coefficient stabilizes [23].

In the last step, a braking system based on an ESD coated C45 steel substrate was simulated. The braking system using ESD coatings as a friction material achieves the best result of the braking distance among all performed simulations. When braking from a speed of 10 m/s, the AGV traveled a distance of 4.07 m until it came to a total stop. The time required for a total stop was less than 1 s (Fig. 17a). As a conclusion, it can be stated that the coated C45 steel substrate showed the best results of the braking distance and braking time.

As can be seen in Fig. 18b the optimal ratio of composition of the WC-Cu coating resulted high friction factor. It is assumed that by choosing the right ratio of composition of WC-Cu coating, the brake system will perform its function similarly well as brake systems based on metallic or ceramic friction materials. Moreover, if the coating wears out, the worn surface can be repaired again by ESD technology.

6. Simulation of heat flow in a brake system

In addition to the mechanical properties, the thermal properties of the brake system must be taken into account in the

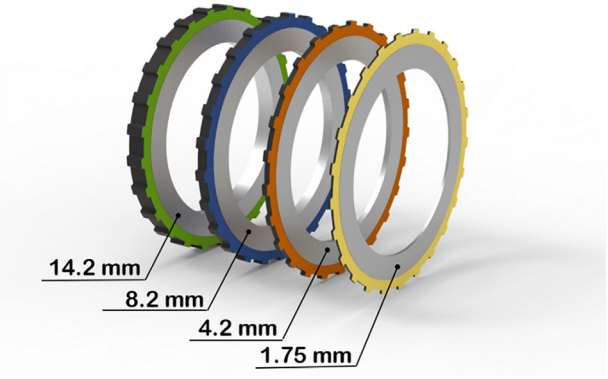

Fig. 19 – Steel Discs for considering brake system [authors].

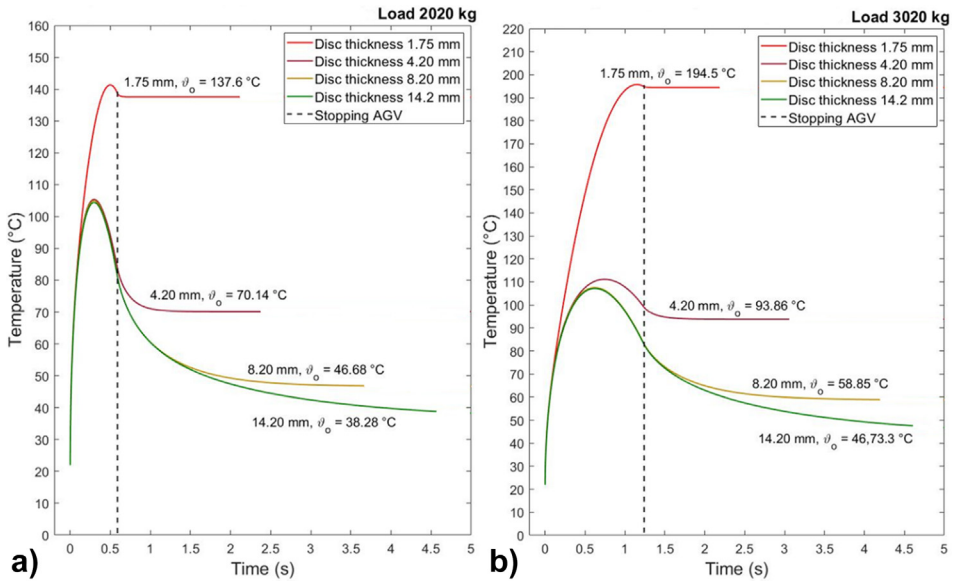

Fig. 20 – Temperature profile during braking with a load of 2020 kg (a), 3020 kg (b).

design phase of the brake system of every vehicle [24]. The methods of testing and simulating the heat flow are described also in [25,26]. During braking, mechanical energy is converted into thermal energy. The heat generated during braking accumulates both in the steel friction discs and in ESD coated discs. Also, the produced heat spreads from the brake system to the whole wheel. This is not the case with brake systems based on ceramic or metallic friction material. In this case, the heat produced is not absorbed into the friction material but only into the steel discs. In general, it is significant for brake systems that their elements cool down quickly enough. Overheating reduces the efficiency of the entire system. In the automotive industry, are used brake discs on the front axle, which have ventilated construction of disc. Some car models use vents in the front bumpers, which primarily ensure more efficient airflow to the brake disc and secondary create a sporty design element. The AGV brake system has been integrated in the enclosed interior of the drive wheel, so it must cool down quickly enough after braking. The theory of physics speaks for itself. Thinner thicknesses of steel discs absorb large amounts of heat extremely quickly during braking. This is not the case with thicker steel disc. Larger disk thicknesses are not sufficient to absorb the large amount of heat produced in a shorter period of time and therefore cool quickly enough. For this reason, it is necessary to determine the optimal thickness of the steel disc to meet the thermodynamics and design requirements. For this reason, the braking system is subjected to a simulation of the heat flow on the surface of the steel disc during AGV braking. The simulation is set for two operating modes with four different thicknesses of steel disc (Fig. 19). Publications focused on thermodynamics of brake systems state that a friction material based on metal and ceramics has a low coefficient of thermal conductivity. As a result, there is no significant heat absorption into the brake pad during the braking process.

In the case of investigated brake system, the construction which consists of a ESD coated C45 steel substrate, the same heat absorption takes place as with the base material before coating. The ESD technology did not affect the original physical and mechanical properties of the material. Therefore, the same heat accumulates in both types of discs (Spacers and Washers) in the brake system. Using the simulation, the heat flow during the single braking of the AGV was investigated considering several thicknesses of steel discs from 1.75, 4.2, 8.2–14.2 mm (Fig. 19).

The simulation was done using the Matlab® calculation program, where the mathematical notation (script) was formed by a derived Fourier partial differential equation for non-stationary heat conduction (Eq. (6)) [26–29]. The simulation is set for both load operating modes. In the first operating mode, the discs have warmed up to a lower temperature as expected. The obtained results show that for the mentioned operating conditions it is more suitable to use a brake system with a disc thickness ranging from 8.2 to 14.2 mm (Fig. 20). In the second operating mode, the 14.2 mm thick disc absorbed a temperature of 46 °C after braking. The 8.2 mm thick disc

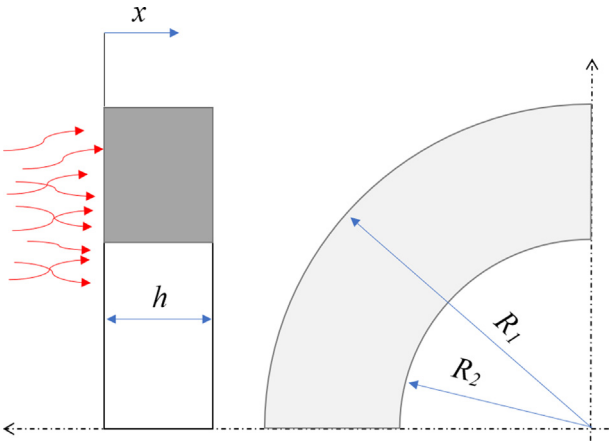

Fig. 21 – Cross-section of steel disc [30].

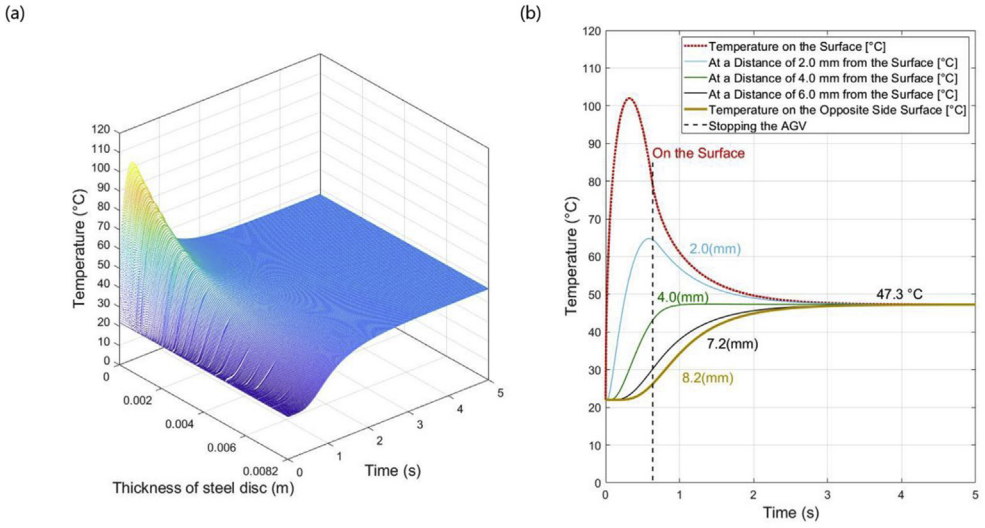

Fig. 22 – Temperature profile in a specific cross-section of the disc (8.2 mm) (a), three-dimensional representation (b).

absorbed at the same settings a temperature of 58 °C, which is about 12 °C more than in the previous case. The difference in the absorbed temperature between the two discs is not large, but a fundamental difference occurs in the size and weight of the disc. The geometric shape and weight of the disc have major impact on the overall design of the brake system. For this reason, it was necessary to further examine the heat flow in the cross-section of both discs at the time of braking and then evaluate the suitability of their use in the considered brake system.

$$\frac{\vartheta_p}{\vartheta_o}=\frac{2.t^*}{t_b}.\left(1-\frac{t^*}{2.t_b}\right)+\frac{4}{\pi^2}.G.\sum_{m=1}\frac{1}{m^2}.\left[\left(1+\frac{G}{m^2.\pi}-\frac{t^*}{t_b}\right).e^{-\frac{m^2.\pi^2}{G}.\left(\frac{t}{t_b}-\frac{t^*}{t_b}\right)}-\left(1+\frac{G}{m^2.\pi}\right).e^{-\frac{m^2.\pi^2}{G}.\frac{t}{t_b}}\right] \quad (6)$$

6.1. 3D simulation of heat flow

Simulation of the heat flow during AGV braking shows that discs with a thickness in the range 8.2–14.2 mm give thermodynamic results acceptable for the concept of the considered brake system. Subsequently, discs with thickness of 8.2 and 14.2 mm were subjected to 3D simulations, in order to examine in more detail, the course heat flow on the surface and in the cross-section of the discs. At the beginning of the brake system design process, several design and operational requirements (boundary conditions) were set. One condition concerns proportional size of the brake system, as the space for integration into the drive wheel is limited. A disc with a thickness of 8.2 mm has several advantages over a disc thickness of 14.2 mm.

In terms of size and weight ratio, the disc is satisfactory, but it is also important to think about the thermodynamic

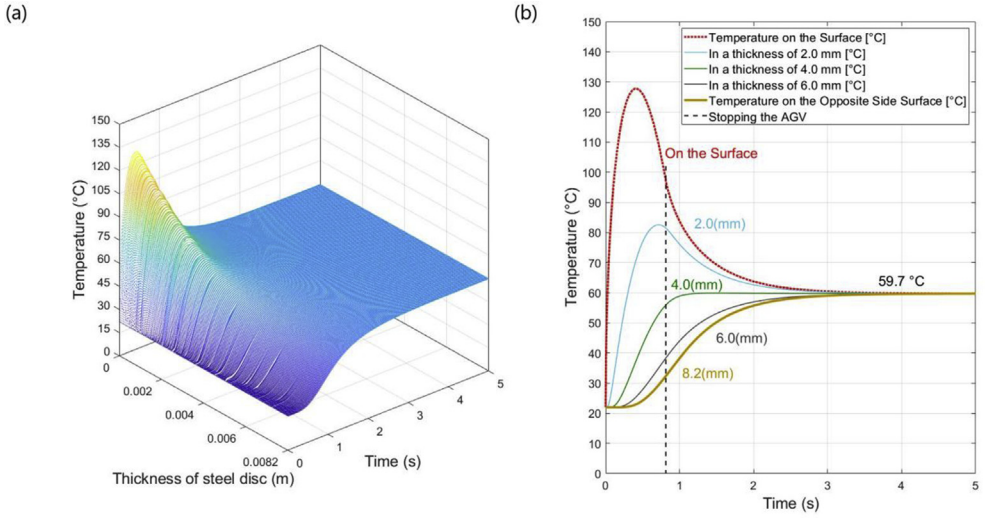

Fig. 23 – Temperature profile in a specific cross-section of the disc (8.2 mm) (a), three-dimensional representation (b).

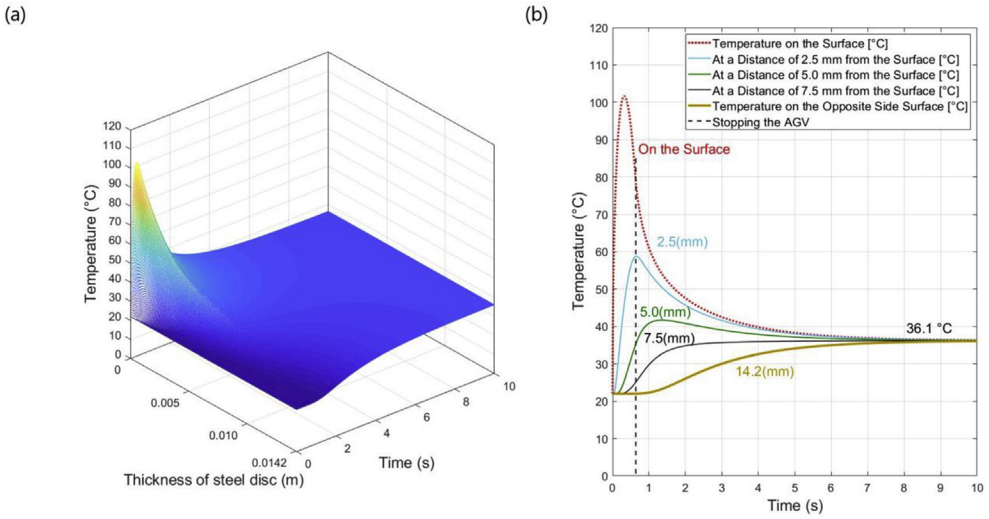

Fig. 24 – Temperature profile in a specific cross section of the disc (14.2 mm) (a), three-dimensional representation (b).

properties during braking. As in the previous chapter, a 3D heat flow simulation was done using Matlab® computational software using a Fourier partial differential equation for non-stationary heat conduction (Eq. (7)) [27–30].

Eq. (7) is based on a mathematical relation to calculate the surface temperature of the disc (6). The difference between the equations was made by adding a third coordinate, which represents the thickness of the disc (symbol - h). The symbol "x" given in Eq. (7) represents the distance of a particular cross-section from the surface of the steel disc, where the value of the accumulated heat was examined [30]. The symbol "h" indicates the thickness of the steel disc (Fig. 21). In this case, the same boundary conditions are valid as for the mathematical relationship given by Eq. (6) [30]. The first two diagrams present the heat flow in a brake system with an 8.2 mm thick steel disc. In the first operating mode (2020 kg), the temperature on the surface of the disc reached a value of over 100 °C (Fig. 22). Ultimately, the heat received by the brake system after a single brake is 47.3 °C. The diagram also shows the temperature in specific sections of the disc. In the second operating mode, the surface temperature of the disc rose to almost 130 °C (Fig. 23). At this setting, the brake system absorbed a temperature of 59.7 °C. In view of the obtained results, it can be stated that the difference in the absorbed temperature between the first and the second operating mode increased by 26.2%. The stated results are satisfactory within the design solution of the brake system.

$$\frac{\vartheta_{(x,t)}}{\vartheta_o} = \frac{2.t^*}{t_b}.\left(1-\frac{t^*}{2.t_b}\right) + \frac{4}{\pi^2}.G.\sum_{m=1}\frac{\cos\left(m.\pi.\frac{x}{h}\right)}{m^2}. \left[\left(1+\frac{G}{m^2.\pi}-\frac{t^*}{t_b}\right).e^{-\frac{m^2.\pi^2}{G}.\left(\frac{t}{t_b}-\frac{t^*}{t_b}\right)} - \left(1+\frac{G}{m^2.\pi}\right).e^{-\frac{m^2.\pi^2}{G}.\frac{t}{t_b}}\right] \quad (7)$$

The last two diagrams (Figs. 24 and 25) express the results of the simulation of the heat flow in the brake system, the construction of which consists of discs with a thickness of

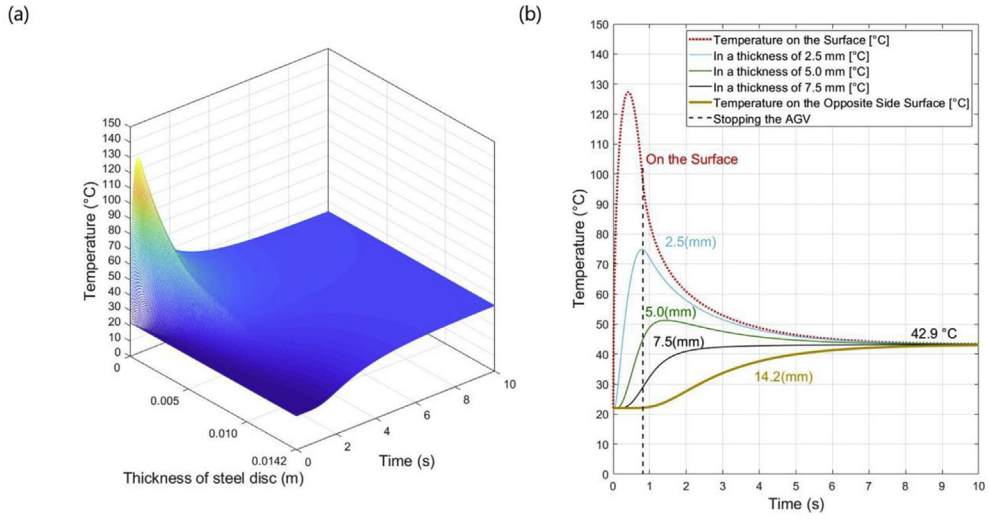

Fig. 25 – Temperature profile in a specific cross section of the disc (14.2 mm) (a), three-dimensional representation (b).

14.2 mm. In both operating modes, the braking system received less heat during braking as expected than in the case of a braking system with a disc thickness of 8.2 mm. In the case of the first operating mode, the temperature in the brake system reached a value of 36.1 °C (Fig. 24). In the second operating mode, the temperature rose to 42.9 °C, which represents an increase of 18.83% (Fig. 25). It should be noted that from a physical point of view, a larger volume of steel cannot be heated to a high temperature in a short time. For this reason, this design of the brake system shows more acceptable thermodynamic results than a brake system with a disc thickness of 8.2 mm.

The results of simulation of braking system with a disc thickness of 8.2 mm also show that this braking system will be sufficient for the considered operating modes. During the process of computer design of the brake system, the engineer has to think also about venting the enclosed space of the brake system. The brake housing must be provided with ventilation of the heat generated during braking. Many qualified publications deal with this issue, such as [31]. During the design process, it is essential to keep in mind that covers made of aluminium alloys can block the ventilation of the heat produced from the brake system space [32].

7. Conclusions and discussion

The experimental research contained in this paper describes the investigation of the thermodynamic and tribological properties of the C45 steel substrate. Three pairs of samples were prepared by machining from the C45 steel and then subjected to a pulsed micro-welding process using the ESD technology. Different electrodes were used for the electrospark deposition, resulting in different chemical compositions of the ESD coatings. The percentage composition of tungsten carbide (WC) and copper (Cu) was chosen in the first sample in the ratio WC80–Cu20, in the second case WC50–Cu50 and in the last sample WC20–Cu80. The surface of ESD coatings has a very rough character. More favorable quality of the ESD coatings can be obtained using laser post treatment. In the publications [17–19], the authors describe their research, in which they focused on the post-treatment of ESD coatings by laser remelting. During their research, they came to very favorable results. Laser remelting of ESD coatings was applied as a post treatment also in our study. In our experimental study, laser remelting was applied to the samples with ESD coatings and also to the samples without ESD coating. After the laser post treatment, the ESD coatings obtained a visibly more uniform and smoother surface character. On the other hand, as verified in publications [17–19] laser post-treatment slightly reduced the hardness of the treated materials. In this case the influence of laser post treatment on the hardness of the C45 steel substrate was negligible but the hardness of ESD coatings after laser post treatment was significantly lower.

The experimental investigation of the friction factor of ESD coatings with variable WC-Cu ratio has shown that the ratio of chemical elements significantly affects the friction factor and the duration of the coating. A significantly higher ratio of copper (80% Cu) in the coating structure causes soft spots that have been manifested themselves in fluctuation of the friction factor curve. However, it should be noted that coatings with a higher percentage of copper (Cu) achieve a higher friction factor. Otherwise, when the sample contained a smaller ratio of copper (20% Cu), the surface was so hard that it would cause large vibrations in the brake system during braking. It can be stated that a higher ratio of tungsten carbide (WC) adds higher wear resistance to the coating. In both diagrams, the curve for the friction factor of the WC80–Cu20 coating has the shape of a dense oscillating curve. Our research demonstrated that the combination of 50% WC and 50% Cu shows an optimal balance between wear and friction factor. Using this ratio of WC and Cu in the ESD coating it is possible to achieve an optimal result.

Samples with ESD coatings were also subjected to braking simulations. Commercial friction materials based on metal, ceramic and organic friction material were chosen to compare the friction properties of ESD coatings.

Results of the simulation of AGV braking shows that the difference between the braking time for individual braking systems is very low, nearly negligible. The difference occurs in the trajectory that the individual AGVs take during braking. There is a 3.0 m difference in braking distance between the organic material and the ESD-coated C45 steel substrate, which is no longer a negligible parameter.

By simulating the heat flow in the brake system during AGV braking, it was found that the considered disc thicknesses of 8.2 and 14.2 mm do not absorb a large amount of heat under the given operating conditions. A more detailed examination concluded that the disc with a thickness of 8.2 mm is optimal for the given solution of the brake system. Results of the 3D simulation also show that short-term exposure to heat flow affects strongly the area of the disc, which is located a few millimetres from the friction surface. This aspect appeared in both simulated discs. It should be added that the disc with a thickness of 14.2 mm absorbed about 10–12% less heat under the given operating conditions, but it is unsatisfactory in terms of the requirements of the developed brake system. Its total weight and thickness put it in the second place.

Several highly qualified publications reported that WC-Cu coatings create a very durable surface. In case of mechanical damage of ESD coating it can be repaired again using the ESD technology. This fact puts this ESD technology in a competitive position. Restoration of the friction surface with the same technological procedure is not possible with commercial brake pads based on ceramic, metallic or organic friction material. When maintaining brake systems that use commercial friction materials, it is necessary to replace the entire brake pad segment. This aspect disappears with application of ESD coatings. Braking comfort connected with application of ESD friction coatings remains still unexplored. Aspect of the braking comfort can only be verified by real experiments. Another advantage of the ESD friction coatings is their almost constant course of the friction coefficient. During the development of the brake system, great emphasis was placed on the safe distance of the braking distance and operational safety. Another important requirement was the reliability and efficiency of the entire braking system. Copper is a corrosion resistant material with high heat conductivity. Moreover, as a

coating material, it reduces the residual (tensile) stresses and improves adhesion [33,34]. The use of the WC-Cu coating in brake systems will make the copper act as a solid lubricant. The issue of manufacturing new materials based on WC and Cu and the search for their applications is of topical interest to many researchers [35,36]. In their works, the authors presented WC-Cu sinters made using hot pressing. WC-Cu cermet's were devised for thermal barriers between the plasma facing tungsten tiles and the copper-based heat sink in the first wall of nuclear fusion reactors [36]. The aim of the research contained in the paper was to achieve, through additional laser beam machining (LBM), an enhancement of the performance characteristics of ESD-made WC-Cu coatings that should lead to the reduction of structural defects and adhesion improvement. The rationale of selecting an investigation approach was to point out the most appropriate ESD electrode composition considering the subsequent processing phase, i.e., LBM. Regardless, the particular detailed results and obtained model could be of practical interest for specific R&D and industrial applications, for example, brake materials. Further investigation should result in a more precise model and reveal possible new technological factors of significant influence. Finally, it should be noted that all copper compounds (e.g. Cu0 or Cu_20) should be considered as a little bit toxic for the human body and bacterial flora but harmless for the plants. Mankind has used copper and its alloys since time immemorial. Ancient kitchenware and copper roofs are proof of this. Copper roofing oxidizes and during the rain, copper oxide flows into the ground and nature seems to be able to deal with copper. However, the design of the brake system is closed into the wheel and the brake dust is kept inside the brake system throughout the operation of the AGV. During the friction of WC-Cu coatings, a minimum amount of dust is generated and it is assumed that this amount will not have an adverse effect on the environment and human health.

Declaration of Competing Interest

The authors declare that they have no known competing financial interests or personal relationships that could have appeared to influence the work reported in this paper.

Acknowledgement

This publication was realized with support of Operational Program Integrated Infrastructure 2014–2020 of the project: Innovative Solutions for Propulsion, Power and Safety Components of Transport Vehicles, code ITMS 313011V334, co-financed by the European Regional Development Fund; KEGA 026 ŽU – 4/2019 and Grant System of University of Zilina No. 1/2020. (7879).

REFERENCES

[1] Mruzek M, Gajdac I, Kucera L, Gajdosik T. The possibilities of increasing the electric vehicle range. TRANSCOM: International scientific conference on sustainable, modern and safe transprt. Procedia Eng 2017;192:621–5.

[2] Kucera L, Gajdosik T, Gajdac I, Mruzek M, Tomasikova M. Simulation of real driving cycles of electric cars in laboratory conditions. Communications - Scientific Letters of the University of Zilina 2017;19(2A):42–7.

[3] Varecha D, Kohar R, Gajdosik T. Optimizing the braking system for handling equipment. In: 9th international scientific conference – IRMES. 659. IOP Publishing Ltd; 2019. p. 1–10. Sep 5-7; Kragujevac, Serbia. (IOP Konf. Ser.: Mater. Sci. Angl. 659 012062).

[4] Weis P, Kucera L, Pechac P, Mocilan M. Modal analysis of gearbox housing with applied load. Procedia Eng 2017;192:953–8.

[5] Steininger J, Hrcek S, Smetanka L, Skyba R. Optimisation procedure of inner geometry in spherical roller bearings with regard to their durability. Sci J Sil Univ Technol Series Transp 2020;106:173–81. https://doi.org/10.20858/sjsutst.2020.106.15.

[6] Steininger J, Hrcek S, Gajdosik T, Stopka M. The optimization procedure of the inner geometry in the spherical roller bearings with regard to their durability. In: Proceedings of 58th international conference of machine design departments, 2017 Sep 6-8; 2017. p. 352–5. Prague, Czech republic.

[7] Skyba R, Hrcek S, Smetanka L, Majchrak M. Strength analysis of slewing bearings. Transp. Res. Procedia. 2019;40:891–7. https://doi.org/10.1016/j.trpro.2019.07.125.

[8] Belorit M, Hrcek S, Gajdosik T, et al. Description of the bearing check program for countershaft gearboxes. In: Proceeding of 58th international conference of machine design departmens (ICDM), 2017 sep 6-8; 2017. p. 32–5. Prague, Czech republic.

[9] Kraus V. Vypocet teplot radiacich lamelovych spojok a brzd (Calculation of temperature multi-disc shifting brake and shifting clutches). Habitation thesis. Žilina: Edis; 1980 [in Slovak].

[10] United States Patent. Organic friction material. Owner and originator of the patent: fujimaku et al., Pat. No. 4,451,590A. 1984. May 29.

[11] Seydibeyoglu MÖ, Mohanty AK, Misra M. Fiber technology for fiber-reinforced composites. Woodhead Publishing; 2017. p. 153–67.

[12] Begelinger A, de Gee A. A new method for testing brake lining materials. In: Thiruvengadam A, editor. Erosion wear, and interfaces with corrosion. West Conshohocken, PA: ASTM International; 1974. p. 316–34.

[13] Huang L, Huang L, Yafei L, Ling H, Zhang J. Optimization of ceramic friction materials. Compos Sci Technol 2006;66(15):2895–906. https://doi.org/10.1016/j.compscitech.2006.02.027.

[14] Brumercik F, Bastovansky R, Lukac M, Glowacz A. Molybdenum strip test experiments and simulations at various temperatures to determine friction coefficients. Measurement 2021:172. https://doi.org/10.1016/j.measurement.2020.108859.

[15] Homepage Porsche. Technical article: Porsche surface coated brakes [homepage on the internet]. Jalan Sungai Besi, Kuala Lumpur, Malaysia. 2021 [cited 2021 Jun 8]. Available from: https://dealer.porsche.com/my/sungaibesi/en-GB/Offers/Technical-article-porsche-surface-coated-brakes-519.

[16] Homepage Porsche–Technical article: Hard like Diamond [homepage on the internet]. Zuffenhausen, Germany [cited 2021 Jun 8]. Available from: https://www.porsche.com/international/aboutporsche/christophorusmagazine/archive/384/articleoverview/article03/.

[17] Radek N, Bartkowiak K. Performance properties of electro-spark deposited carbide – ceramic coating modified by laser beam. Physics Procedia 2010;5(5A):417–23. https://doi.org/10.1016/j.phpro.2010.08.163.

[18] Radek N, Pietraszek J, Gadek-Moszczak A, Orman LJ, Szczotk A. The morphology and mechanical properties of ESD coatings before and after Laser Beam Machining. Materials 2020;13(10):2331. https://doi.org/10.3390/ma13102331.
[19] Radek N, Szczotok A, Gądek-Moszczak A, Dwornicka R, Broncek J, Pietraszek J. The impact of Laser processing parameters on the properties of electro-spark deposited coatings. Arch Metall Mater 2018;63(2):809–16. https://doi.org/10.24425/122407.
[20] Konstanty J, Radek N, Scendo M. The electro-spark deposited WC-Cu coatings modified by laser treatment. Arch Metall Mater 2015;60(4):2579–84. https://doi.org/10.1515/amm-2015-0417.
[21] Ho SC, Lin Chern JH, Ju CP. Effect of carbonization on mechanical and tribological behavior of a copper–phenolic-based friction material. Carbon 2005;43(3):491–502. https://doi.org/10.1016/j.wear.2004.12.029.
[22] Tomasikova M, Tropp M, Gajdosik T, Krzywonos L, Brumercik F. Analysis of transport mechatronic system properties. Procedia Eng 2017;192:881–6. https://doi.org/10.1016/j.proeng.2017.06.152.
[23] Orlowic AW, Mroz M, Wnuk G, Markowska O, Homik W, Kolbusz B. Coefficient of friction of a brake disc-brake pad friction couple. Arch Foundry Eng 2016;16(4):196–200. https://doi.org/10.1515/afe-2016-0109.
[24] Milenkovic DP, et al. The influence of brake pads thermal conductivity on passenger car brake system efficiency. Therm Sci 2010;14(Supl):221–30. https://doi.org/10.2298/TSCI100505016M.
[25] Mitka M, Bastovansky R, Brumercik F, Ignaciuk P. Local resistance of heating molybdenum sheet in a test device. Adv Sci Technol Res J 2017;11(3):87–93. https://doi.org/10.12913/22998624/74182.
[26] Tropp M, Tomasikova M, Bastovansky R, Krzywonos L, Brumercik F, Krzysiak Z. Transient thermal simulation of working components of mechatronic system for deep drawing of molybdenum sheets. In: Proceedings of 58th international conference of machine design departments (ICMD), 2017 Sep 6-8; 2017. p. 408–13. Prague, Czech republic.
[27] Siedlecka U. Heat conduction in the finite medium using the fractional single-phase-lag model. Bull Pol Acad Sci Tech Sci 2019;67(2):401–7. https://doi.org/10.24425/bpas.2019.128599.
[28] Spałek D. Two relations for generalized discrete fourier transform coefficients. Bull Pol Acad Sci Tech Sci 2018;66(3):275–81. https://doi.org/10.24425/123433.
[29] Wolf KB. Integral transforms in science and engineering. 1st ed. Boston, MA: Fourier Transforms; 1979. p. 255–378 [Chapter 7].
[30] Varecha D, Kohar R, Lukac M. Theoretical study of heat conduction in the multi-disc brake integrated into the drive wheel AGV during braking. Bull Pol Acad Sci Tech Sci 2021;69(2):e136718. https://doi.org/10.24425/bpasts.2021.136718.
[31] Muszynsky T, Kozieł SM. Parametric study of fluid flow and heat transfer over louvered fins of air heat pump evaporator. Arch Therm 2016;37(3):45–62. https://doi.org/10.1515/aoter-2016-0019.
[32] Nia Bassiri A, Nejad Farokhi A, Xin L, Ayob A, Yahya Yazid M, Koloor Seyed Rahimian S, et al. Dynamic response of aluminium sheet 2024-T3 subjected to close-range shock wave: experimental and numerical studies. J Mater Res Technol 2021;10(Jan-Feb):349–62. https://doi.org/10.1016/j.jmrt.2020.12.029.
[33] Radek N, Antoszewski B. Influence of laser treatment on the properties of electro-spark deposited coatings. Met Mater 2009;47(1):31–8.
[34] Zhao J, Yu DQ, Wang L. Improvement on the microstructure stability, mechanical and wetting properties of Sn-Ag-Cu lead-free solder with the addition of rare earth elements. J Alloys Compd 2004;376(1–2):170–5. https://doi.org/10.1016/j.jallcom.2004.01.012.
[35] Dias M, Guerreiro F, Tejado E, Correia J, Mardolcar U, Coelho M, et al. WC-Cu thermal barriers for fusion applications. Surf Coating Technol 2018;355:222–6. https://doi.org/10.1016/j.surfcoat.2018.02.086.
[36] Tejado E, Dias M, Correia J, Palacios T, Carvalho P, Alves E, et al. New WC-Cu thermal barriers for fusion applications. High temperature mechanical behaviour. J Nucl Mater 2018;498:355–61. https://doi.org/10.1016/j.jnucmat.2017.10.071.